Stochastic GW calculations for molecules

Vojtěch Vlček,[1] Eran Rabani,[2,3,*] Daniel Neuhauser,[1,†] and Roi Baer[4,‡]

[1] *Department of Chemistry and Biochemistry, University of California, Los Angeles California 90095, U.S.A.*[§]
[2] *Department of Chemistry, University of California and Materials Science Division, Lawrence Berkeley National Laboratory, Berkeley, California 94720, USA*
[3] *The Raymond and Beverly Sackler Center for Computational Molecular and Materials Science, Tel Aviv University, Tel Aviv, Israel 69978*
[4] *Fritz Haber Center for Molecular Dynamics, Institute of Chemistry, The Hebrew University of Jerusalem, Jerusalem 91904, Israel*

Quasiparticle (QP) excitations are extremely important for understanding and predicting charge transfer and transport in molecules, nanostructures and extended systems. Since density functional theory (DFT) within Kohn-Sham (KS) formulation does not provide reliable QP energies, a many-body perturbation technique within the GW approximation are essential. The steep computational scaling of GW prohibits its use in extended, open boundary, systems with thousands of electrons and more. Recently, a stochastic formulation of GW has been proposed [*Phys. Rev. Lett.* **113,** 076402 (2014)] which scales nearly linearly with the system size, as illustrated for a series of silicon nanocrystals exceeding 3000 electrons. Here, we implement the stochastic GW (sGW) approach to study the ionization potential (IP) of a subset of molecules taken from the "GW 100" benchmark. We show that sGW provides a reliable results in comparison to GW WEST code and to experimental results, numerically establishing its validity. For completeness, we also provide a detailed review of sGW and a summary of the numerical algorithm.

I. INTRODUCTION

First principles calculations of electronic structure play a central role in predicting and understanding the behavior of molecules, nanostructures and materials. Methods for describing the electronic properties of such systems can be divided into ground or excited state techniques. For the ground state density functional theory,[1,2] Hartree–Fock (HF) method, and to some extent post HF techniques such as Møller–Plesset perturbation theory are the methods of choice. Calculation of the ground state properties of extended, finite systems is routinely possible mainly due to expeditious numerical implementations of electronic structure solvers along with the increase in computational power (see Ref. 3 and references therein).

For charge (quasiparticle) and neutral (optical) excitations, the situation is more complex, and most if not all methods are limited to either small molecules or to periodic crystals with a relatively small unit cell.[4–14] While DFT is a theory for the ground state, recent developments using hybrid functionals,[15–17] extend the use of DFT to describe QP excitations, even in system with thousands of electrons.[18] However, the description of the QP excitations within the DFT hybrids lacks dynamical effects, such as screening and lifetime of the QPs.

An alternative for describing excitations is based on many-body perturbation techniques, within the GW approximation[19–24] for QPs and the Bethe-Salpeter equation (BSE) for neutral excitations.[23,25–27] Both approaches are limited to rather small system sizes. Recently, we have developed a stochastic approach for both flavors, the so called stochastic GW (sGW)[28] and the stochastic Bethe-Salpeter equation (sBSE) approach.[29] The former method scales near-linearly while the latter scales quadratically with system size. While both stochastic methods extend significantly the size of systems that can be studied within many-body perturbation techniques, only the sGW is fully *ab initio* and thus, can be compared to other GW formulations.

The purpose of this paper is to compare the sGW approach with a state of the art deterministic method, namely the WEST code[13] implementation of GW for a representative subset of the "GW 100" set of molecules.[30] For completeness in Section II we review the sGW formalism and provide a summary of the algorithm.[28] In Section III we summarize the results for the subset of GW 100 molecules. Summary and conclusions are presented in Section IV.

II. STOCHASTIC FORMULATION OF THE G_0W_0 APPROXIMATION

A. G_0W_0 in the energy domain

It is possible to write a formal equation for the QP Dyson orbitals $\psi_n^{QP}(\boldsymbol{r})$ and energies ε_n^{QP}:

$$-\frac{\hbar^2}{2m_e}\nabla^2\psi_n^{QP}(\boldsymbol{r})+v_{\rm ext}(\boldsymbol{r})\,\psi_n^{\rm QP}(\boldsymbol{r})+v_{\rm H}(\boldsymbol{r})\,\psi_n^{QP}(\boldsymbol{r})+\int\tilde{\Sigma}\left(\boldsymbol{r},\boldsymbol{r}',\varepsilon_n^{QP}\right)\psi_n^{QP}(\boldsymbol{r}')\,{\rm d}\boldsymbol{r}'=\varepsilon_n^{QP}\psi_n^{QP}(\boldsymbol{r}) \qquad (1)$$

which is similar to a Schrödinger equation, containing kinetic energy and external potential energy ($v_{\text{ext}}(\boldsymbol{r})$) operators as well as a mean electrostatic or Hartree potential

$$v_{\text{H}}(\boldsymbol{r}) = \int n(\boldsymbol{r}')\, u_C(|\boldsymbol{r}-\boldsymbol{r}'|)\, d\boldsymbol{r}', \tag{2}$$

where $n(\mathbf{r})$ is the ground-state density of the N-electron system and $u_C(r) = \frac{e^2}{4\pi\epsilon_0 r}$ is the bare Coulomb potential energy. This equation also contains a non-local energy-dependent self-energy term $\tilde{\Sigma}(\boldsymbol{r},\boldsymbol{r}',\omega)$ which encompasses the many-body exchange and correlation effects into the system. Eq. (1) is exact, but requires the knowledge of the self-energy which cannot be obtained without imposing approximations. One commonly used approach is based on the GW approximation.[19] However, even this theory is extremely expensive computationally and a further simplification is required leading to the so-called G_0W_0 approximation

$$\tilde{\Sigma}(\boldsymbol{r},\boldsymbol{r}',\omega) = i\int_{-\infty}^{\infty}\frac{d\omega'}{2\pi}\tilde{G}_0(\boldsymbol{r},\boldsymbol{r}',\omega+\omega')\,\tilde{W}_0(\boldsymbol{r},\boldsymbol{r}',\omega'). \tag{3}$$

$\tilde{G}_0(\mathbf{r},\mathbf{r}',\omega)$ is a time-ordered Green's function given by:

$$\tilde{G}_0(\boldsymbol{r},\boldsymbol{r}',\omega) = \lim_{\eta\to 0^+}\hbar\sum_n \phi_n^{KS}(\mathbf{r})\,\phi_n^{KS}(\mathbf{r}')\left[\frac{f_n}{\hbar\omega-\varepsilon_n^{KS}-i\eta}+\frac{1-f_n}{\hbar\omega-\varepsilon_n^{KS}+i\eta}\right], \tag{4}$$

within a Kohn-Sham (KS) DFT starting point.[1,2] $\phi_n^{KS}(\mathbf{r})$ and ε_n^{KS} are the real KS eigenstates and eigenvalues, respectively, of the KS Hamiltonian (we use atomic units where $\hbar = m_e = e = 4\pi\epsilon_0 = 1$)

$$\hat{h}_{KS} = -\frac{1}{2}\nabla^2 + v_{\text{ext}}(\boldsymbol{r}) + v_{\text{H}}(\boldsymbol{r}) + v_{\text{xc}}(\boldsymbol{r}), \tag{5}$$

and $v_{\text{xc}}(\boldsymbol{r})$ is the exchange-correlation potential that depends on the ground state density, $n(\boldsymbol{r})$. In Eq. 4, f_n is the occupation of the KS level n. In Eq. (3), $\tilde{W}_0(\boldsymbol{r},\boldsymbol{r}',\omega')$ is the *time-ordered* screened Coulomb potential defined as

$$\tilde{W}_0(\boldsymbol{r},\boldsymbol{r}',\omega) = \int \epsilon^{-1}(\boldsymbol{r},\boldsymbol{r}'',\omega)\, u_C(|\boldsymbol{r}''-\boldsymbol{r}'|)\, d\boldsymbol{r}'', \tag{6}$$

where $\epsilon^{-1}(\boldsymbol{r},\boldsymbol{r}',\omega) = \delta(\boldsymbol{r}-\boldsymbol{r}') + \int u_C(|\boldsymbol{r}-\boldsymbol{r}''|)\,\tilde{\chi}(\boldsymbol{r}'',\boldsymbol{r}',\omega)\,d\boldsymbol{r}''$ is the frequency dependent inverse dielectric function and $\tilde{\chi}(\boldsymbol{r},\boldsymbol{r}',\omega)$ is the reducible polarizability.

Once the self-energy is generated via Eqs. (3)--(6) the QP energies of Eq. (1) can be estimated perturbatively, as a correction to the KS orbital energies. To first order:[20,21]

$$\varepsilon_n^{QP} = \varepsilon_n^{KS} - V_{XC} + \tilde{\Sigma}_n\left(\varepsilon_n^{QP}\right), \tag{7}$$

where $V_{XC} = \int v_{XC}(\boldsymbol{r})\left|\phi_n^{KS}(\boldsymbol{r})\right|^2 d\boldsymbol{r}$ is the average exchange-correlation energy, and $\tilde{\Sigma}_n(\omega)$ is the self energy expectation value at a frequency ω:

$$\tilde{\Sigma}_n(\omega) = \iint \phi_n^{KS}(\boldsymbol{r})\,\tilde{\Sigma}(\boldsymbol{r},\boldsymbol{r}',\omega)\,\phi_n^{KS}(\boldsymbol{r}')\,d\boldsymbol{r}d\boldsymbol{r}'. \tag{8}$$

B. G_0W_0 in the time domain

The computational challenge of G_0W_0 is to estimate the frequency-dependent function $\tilde{\Sigma}_n(\omega)$ involving integration over 6-dimensional quantities. A simplification can be achieved if we Fourier transform to the time domain

$$\Sigma_n(t) \equiv \int_{-\infty}^{\infty}\tilde{\Sigma}_n(\omega)\,e^{-i\omega t}\frac{d\omega}{2\pi}. \tag{9}$$

One advantage of the time domain approach is that the self-energy can be expressed in terms of a *product* of the time domain Green's function and screened potential

$$\Sigma(\boldsymbol{r},\boldsymbol{r}',t) = iG_0(\boldsymbol{r},\boldsymbol{r}',t)\,W_0\left(\boldsymbol{r},\boldsymbol{r}',t^+\right), \tag{10}$$

instead of the convolution in Eq. (3). In Eq. (10), t^+ is a time infinitesimally later than t and $G_0(\boldsymbol{r},\boldsymbol{r}',t)$ is the Fourier transform of $\tilde{G}_0(\boldsymbol{r},\boldsymbol{r}',\omega)$, given by:

$$iG_0(\boldsymbol{r},\boldsymbol{r}',t)=\sum_n \phi_n^{KS}(\boldsymbol{r})\,\phi_n^{KS}(\boldsymbol{r}')\,e^{-i\varepsilon_n t/\hbar}\left[(1-f_n)\,\theta(t)-f_n\theta(-t)\right]. \tag{11}$$

The time domain screened potential $W_0(\boldsymbol{r},\boldsymbol{r}',t)$ is the potential at point $\boldsymbol{r}$ and time t of a QP introduced at time $t=0$ at point $\boldsymbol{r}'$. Hence it is composed of an instantaneous Coulomb term and a time dependent polarization contribution:

$$W_0(\boldsymbol{r},\boldsymbol{r}',t)=u_C(|\boldsymbol{r}-\boldsymbol{r}'|)\,\delta(t)+W_P(\boldsymbol{r},\boldsymbol{r}',t). \tag{12}$$

$W_P(\boldsymbol{r},\boldsymbol{r}',t)$ is the polarization potential of the density perturbation due to the QP:

$$W_P(\boldsymbol{r},\boldsymbol{r}',t)=\iint u_C(|\boldsymbol{r}-\boldsymbol{r}''|)\,\chi(\boldsymbol{r}'',\boldsymbol{r}''',t)\,u_C(|\boldsymbol{r}'''-\boldsymbol{r}'|)\,d\boldsymbol{r}''d\boldsymbol{r}''', \tag{13}$$

which is given in terms of the time-ordered reducible polarization function $\chi(\boldsymbol{r},\boldsymbol{r}',t)$. Using these definitions we write the self energy expectation value as a sum of instantaneous and time-dependent contributions:

$$\Sigma_n(t)=\Sigma_n^X\delta(t)+\Sigma_n^P(t). \tag{14}$$

Here, the instantaneous contribution is

$$\Sigma_n^X=-\iint \phi_n^{KS}(\boldsymbol{r})\,u_C(|\boldsymbol{r}-\boldsymbol{r}'|)\,\rho^{KS}(\boldsymbol{r},\boldsymbol{r}')\,\phi_n^{KS}(\boldsymbol{r}')\,d\boldsymbol{r}d\boldsymbol{r}', \tag{15}$$

i.e., the expectation value of the exact exchange operator, where

$$\rho^{KS}(\boldsymbol{r},\boldsymbol{r}')=-iG_0\left(\boldsymbol{r},\boldsymbol{r}',0^-\right)=\sum_n f_n\phi_n^{KS}(\boldsymbol{r})\,\phi_n^{KS}(\boldsymbol{r}') \tag{16}$$

is the KS density matrix. Finally, the polarization self-energy is given by the integral

$$\Sigma_n^P(t)=\iint \phi_n^{KS}(\boldsymbol{r})\,iG_0(\boldsymbol{r},\boldsymbol{r}',t)\,W_P\left(\boldsymbol{r},\boldsymbol{r}',t^+\right)\phi_n^{KS}(\boldsymbol{r}')\,d\boldsymbol{r}d\boldsymbol{r}'. \tag{17}$$

Despite the fact that the time-dependent formalism circumvents the convolution appearing in the frequency-dependent domain, the numerical evaluation of $\Sigma_n^P(t)$ is a significant numerical challenge with numerical effort typically scaling proportionally to N^4 or N^5.[8,12,31] This is due to the fact that $G_0(\boldsymbol{r},\boldsymbol{r}',t)$ involves all (occupied and unoccupied) KS orbitals and $W_P(\boldsymbol{r},\boldsymbol{r}',t)$ involves 6-dimensional integrals (Eq. (13)) depending on the reducible polarization function $\chi(\boldsymbol{r}'',\boldsymbol{r}''',t)$.

C. Stochastic G_0W_0

We now explain how stochastic orbitals enable efficient near-linear-scaling calculation of $\Sigma_n^P(t)$.[28] The calculation is performed using a real space 3D Cartesian grid of equally spaced grid points $\boldsymbol{r}_{ijk}=(i\hat{\mathbf{x}}+j\hat{\mathbf{y}}+k\hat{\mathbf{z}})\,h$ is used, where $\hat{\mathbf{x}}$, $\hat{\mathbf{y}}$, and $\hat{\mathbf{z}}$ are unit vectors in the Cartesian x, y and z directions, i, j and k are integers and h is the grid spacing. In the grid representation the application of the Kohn-Sham Hamiltonian $\hat{h}_{KS}$ onto an $\phi_n^{KS}(\boldsymbol{r})$ on the grid can be performed in a near linear-scaling fashion, depending on the way the kinetic energy is applied. For simplicity, we consider equal grid spacing (h) in the x, y, and z directions, but the formalism is equally valid for different spacing along each direction.

We now introduce a real stochastic orbital $\zeta(\boldsymbol{r})$ on the grid assigning *randomly* $+h^{-3/2}$ or $-h^{-3/2}$ with equal probability to each grid point $\boldsymbol{r}$.[32,33] The average of the expectation value (expressed by $\langle\cdots\rangle_\zeta$) of the projection $\langle|\zeta\rangle\langle\zeta|\rangle_\zeta$ is equal to the unit matrix, $\langle\,|\zeta\rangle\langle\zeta|\,\rangle_\zeta=\hat{\boldsymbol{I}}$, resulting in a "stochastic resolution of identity".[34] In practical calculations the expectation values, i.e. averaging over ζ, are estimated using a finite sample of N_ζ random states. According to the central limit theorem this average will converge to the expectation value as $N_\zeta\to\infty$ (for a discussion of the convergence of the stochastic estimates see Sec. III).

Using the stochastic resolution of the identity any operator can be represented as an average over a product of stochastic orbitals, for example for the KS Green's function:

$$iG_0\left(\boldsymbol{r},\boldsymbol{r}',t\right)=\left\langle\ \zeta\left(\boldsymbol{r}'\right)\zeta\left(\boldsymbol{r},t\right)^*\ \right\rangle_\zeta, \tag{18}$$

where $\zeta\left(\boldsymbol{r}\right)=\langle\boldsymbol{r}|\zeta\rangle$ is the random orbital and

$$\begin{aligned}\zeta\left(\boldsymbol{r},t\right)&=\left\langle\boldsymbol{r}|i\hat{G}_0\left(t\right)|\zeta\right\rangle \\ &=\left\langle\boldsymbol{r}|e^{-i\hat{h}_{KS}t/\hbar}\left[\theta\left(t\right)-\theta_\beta\left(\mu-\hat{h}_{KS}\right)\right]|\zeta\right\rangle.\end{aligned} \tag{19}$$

is the G-operated random orbital. Here, μ is the chemical potential, $\theta\left(t\right)$ is the Heaviside function, and $\theta_\beta\left(\varepsilon\right)=\frac{1}{2}\left[1+\mathrm{erf}\left(\beta\varepsilon\right)\right]$ (in the limit $\beta\to\infty$, $\theta_\beta\left(\varepsilon\right)\to\theta\left(\beta\varepsilon\right)$). The application of $i\hat{G}_0\left(t\right)$ to ζ in Eq. (18) is performed using a Chebyshev expansion, taking advantage of the sparsity of the KS Hamiltonian in the real-space grid representation. The Chebyshev series includes a finite number of terms proportional to the ratio of the $\hat{h}_{KS}$ eigenvalue range divided by the occupied-unoccupied eigenvalue gap (see, e.g., Ref. 35,36).

The representation used in Eq. (18) decouples position-dependence on $\boldsymbol{r}$ and $\boldsymbol{r}'$ and eliminates the need to represent $iG_0\left(\boldsymbol{r},\boldsymbol{r}',t\right)$ by all occupied and unoccupied orbitals. The exchange part of the self energy can thus be simplified, by replacing the 6-dimensional integral in Eq. 15 by two 3-dimensional integrals:

$$\Sigma_n^X=-\left\langle\int\phi_n^{KS}\left(\boldsymbol{r}\right)\zeta\left(\boldsymbol{r},0^-\right)v_\zeta^{\mathrm{aux}}\left(\boldsymbol{r}\right)d\boldsymbol{r}\right\rangle_\zeta, \tag{20}$$

where the auxiliary potential is

$$v_\zeta^{\mathrm{aux}}\left(\boldsymbol{r}\right)=\int u_C\left(|\boldsymbol{r}-\boldsymbol{r}'|\right)\zeta\left(\boldsymbol{r}'\right)\phi_n^{KS}\left(\boldsymbol{r}'\right)d\boldsymbol{r}', \tag{21}$$

where $\zeta\left(\boldsymbol{r}\right)$ is *projected* to the occupied subspace using the Chebyshev expansion of $\theta_\beta\left(\mu-\hat{h}_{KS}\right)$as in Eq. (19).

In the same vein, the polarization part of the self-energy is recasted in the following form:

$$\Sigma_n^P\left(t\right)=\left\langle\iint\phi_n^{KS}\left(\boldsymbol{r}\right)\zeta\left(\boldsymbol{r},t\right)^*W_P\left(\boldsymbol{r},\boldsymbol{r}',t\right)\phi_n^{KS}\left(\boldsymbol{r}'\right)\zeta\left(\boldsymbol{r}'\right)d\boldsymbol{r}d\boldsymbol{r}'\right\rangle_\zeta,$$

where ζ' is a stochastic orbital (statistically independent of ζ) used to characterize G_0. Further simplifications can be obtained by inserting yet another, independent, stochastic orbital $\xi\left(\boldsymbol{r}\right)$ using the identity

$$\phi_n^{KS}\left(\boldsymbol{r}\right)\zeta\left(\boldsymbol{r},t\right)^*W_P\left(\boldsymbol{r},\boldsymbol{r}',t\right)=\left\langle\int d\boldsymbol{r}''\phi_n^{KS}\left(\boldsymbol{r}''\right)\zeta\left(\boldsymbol{r}'',t\right)^*\xi\left(\boldsymbol{r}''\right)\xi\left(\boldsymbol{r}\right)W_P\left(\boldsymbol{r},\boldsymbol{r}',t\right)\right\rangle_\xi,$$

allowing for decoupling the two t-dependent functions. As a result, the polarization part of the self-energy is an average over a product of two time-dependent stochastic functions $A_{n\zeta\xi}\left(t\right)$ and $B_{n\zeta\xi}\left(t\right)$:

$$\Sigma_n^P\left(t\right)=\left\langle\ A_{n\zeta\xi}\left(t\right)B_{n\zeta\xi}\left(t\right)\ \right\rangle_{\zeta\xi}, \tag{22}$$

where

$$A_{n\zeta\xi}\left(t\right)=\int\phi_n^{KS}\left(\boldsymbol{r}\right)\zeta\left(\boldsymbol{r},t\right)^*\xi\left(\boldsymbol{r}\right)d\boldsymbol{r} \tag{23}$$

and

$$B_{n\zeta\xi}\left(t\right)=\iint\xi\left(\boldsymbol{r}\right)W_P\left(\boldsymbol{r},\boldsymbol{r}',t\right)\phi_n^{KS}\left(\boldsymbol{r}'\right)\zeta\left(\boldsymbol{r}'\right)d\boldsymbol{r}d\boldsymbol{r}'. \tag{24}$$

Calculating $B_{n\zeta\xi}\left(t\right)$ can be done efficiently using the time-dependent Hartree (TDH) method equivalent to the popular random phase approximation (RPA).

The real-time formulation based on TDH provides a description of the *retarded* $W^r(\boldsymbol{r},\boldsymbol{r}',t)$ rather than the time-ordered $W_P(\boldsymbol{r},\boldsymbol{r}',t)$ needed in Eq. 24. In linear-response, the two functions are simply related through the corresponding Fourier transforms:[37]

$$\tilde{B}_{n\zeta\xi}(\omega) = \mathrm{Re}\tilde{B}^r_{n\zeta\xi}(\omega) + i\,\mathrm{sign}(\omega)\,\mathrm{Im}\tilde{B}^r_{n\zeta\xi}(\omega), \tag{25}$$

where $\tilde{B}^r_{n\zeta\xi}$ is obtained with $W^r(\boldsymbol{r},\boldsymbol{r}',t)$. Consequently, we now provide a formulation for $B^r_{n\zeta\xi}(t)$, based on Eq. (13) (with χ^r replacing χ) and then use Eq. (25) to obtain the corresponding time-ordered function $B_{n\zeta\xi}(t)$. This leads to the following convolution integral for $B^r_{n\zeta\xi}(t)$:

$$B^r_{n\zeta\xi}(t) = \iint \xi(\boldsymbol{r})\, u_C(|\boldsymbol{r}-\boldsymbol{r}'|)\, \Delta n^r_{n\zeta}(\boldsymbol{r}',t)\, d\boldsymbol{r}d\boldsymbol{r}', \tag{26}$$

which is calculated in almost linear scaling (rather than quadratic) using Fast Fourier Transforms for the convolutions. In the above equation, $\Delta n^r_{n\zeta}(\boldsymbol{r},t)$ is formally given by:

$$\Delta n^r_{n\zeta}(\boldsymbol{r},t) = \int \chi^r(\boldsymbol{r},\boldsymbol{r}',t)\, v_{n\zeta}(\boldsymbol{r}')\, d\boldsymbol{r}', \tag{27}$$

with

$$v_{n\zeta}(\boldsymbol{r}') = \int u_C(|\boldsymbol{r}'-\boldsymbol{r}''|)\, \phi^{KS}_n(\boldsymbol{r}'')\, \zeta(\boldsymbol{r}'')\, d\boldsymbol{r}''. \tag{28}$$

In practice, we calculate the density perturbation by taking stochastic orbitals $\eta(\boldsymbol{r})$ which are projected on the occupied space using the Chebyshev expansion of the operator $\theta_\beta\left(\mu-\hat{h}_{KS}\right)$. Each orbital is then perturbed at time zero as follows:

$$\eta_\tau(\boldsymbol{r},0) = e^{-iv_{n\zeta}(\boldsymbol{r})\tau}\theta_\beta\left(\mu-\hat{h}_{KS}\right)\eta(\boldsymbol{r}) \tag{29}$$

where τ is a small-time parameter. In the RPA, the orbital is now propagated in time by a TDH equation similar to the stochastic time-dependent DFT:[38]

$$i\frac{\partial}{\partial t}\eta_\tau(\boldsymbol{r},t) = \hat{h}_{KS}\eta_\tau(\boldsymbol{r},t) + \left(\int \frac{\Delta n^r_{n\zeta}(\boldsymbol{r}',t)}{|\boldsymbol{r}-\boldsymbol{r}'|}d\boldsymbol{r}'\right)\eta_\tau(\boldsymbol{r},t), \tag{30}$$

where

$$\Delta n^r_{n\zeta}(\boldsymbol{r},t) = \frac{1}{\tau}\left\langle |\eta_\tau(\boldsymbol{r},t)|^2 - |\eta_{\tau=0}(\boldsymbol{r},t)|^2 \right\rangle_\eta. \tag{31}$$

D. The algorithm

We summarize the procedure above by the following algorithm for computing the sGW QP energies:

1. Take N_ζ stochastic orbitals $\zeta(\boldsymbol{r})$ and for each of them, take N_ξ stochastic orbitals $\xi(\boldsymbol{r})$. Use Eq. (19) to generate the projected time-dependent orbitals $\zeta(\boldsymbol{r},t)$. Compute Σ^X_n using Eqs. (20)-(21).
2. Generate $A_{n\zeta\xi}(t)$ from Eq. (23) using $\xi(\boldsymbol{r})$ and $\zeta(\boldsymbol{r},t)$.
3. Generate N_η independent stochastic orbitals $\eta(\boldsymbol{r})$ from which, together with $\xi(\boldsymbol{r})$ and $\zeta(\boldsymbol{r})$, generate $B^r_{n\zeta\xi}(t)$ using Eqs. (24)-(31), where $n^r_{n\zeta}(\boldsymbol{r},t)$ is obtained as an average over η.
4. Fourier transform $B^r_{n\zeta\xi}(t) \to \tilde{B}^r_{n\zeta\xi}(\omega)$ and convert to the time-ordered quantity $\tilde{B}_{n\zeta\xi}(\omega)$ using Eq. (25). Fourier transform back $\tilde{B}^{TO}_{n\zeta\xi}(\omega) \to B^{TO}_{n\zeta\xi}(t)$ and calculate, by averaging on ζ and ξ, the polarization self-energy $\Sigma^P_n(t)$ using Eq. (24).
5. Fourier transform $\Sigma^P_n(t) \to \tilde{\Sigma}^P_n(\omega)$ and using this function estimate the QP energy ε^{QP}_n by solving Eq.(7) self-consistently.

III. RESULTS

The GW method based on the local density approximation (LDA) to DFT is applied to a subset of molecules taken from the GW 100 study.[30] For each molecule we have performed an LDA calculation using a real-space grid approach using Troullier-Martins pseudopotential.[39]The DFT orbitals energies were corrected by an sGW calculation of the quasiparticle energy shift. The results were then compared to deterministic GW calculations using the WEST code.[13]

For each molecule we have converged the calculation with respect to the grid spacing h and the number N_ζ of stochastic orbitals $\zeta(\boldsymbol{r})$, and for each of the latter we used $N_\xi = 100$ stochastic orbitals $\xi(\boldsymbol{r})$ and $N_\eta = 8$ stochastic orbitals $\eta(\boldsymbol{r})$ for the TDH calculations. The time t was discretized using a time step of $\Delta t = 0.05$ *a.u.* for both the Green's function calculation as well as the RPA screening. For the former we employed the Chebyshev series with $N_C = 18,000 - 19,000$ and the temperature parameter of $\beta = 200E_h^{-1}$ (see Eq. (19)). For a given value of β, $N_C \approx 2\beta\Delta E$, where ΔE is the eigenvalue range of the KS Hamiltonian. For the latter, the strength of the *perturbation* was controlled by the parameter $\tau = 0.001$ *a.u.* (see Eq. (29)). The remaining parameters (grid spacing and N_ζ) are defined in Table I.

The accuracy and stability of the sGW approach is governed by the stochastic orbitals $\eta(\boldsymbol{r},t)$ propagated in time using Eq. (30), required for describing the induced density perturbation $\Delta n^r_{n\zeta}(\boldsymbol{r},t)$ in Eq. (31). A finite number of stochastic orbitals can be propagated only for a finite time as the response to an external impulse is amplified leading to an instability.[29] When transforming from the time to the frequency domain we use a damping factor, $\tilde{B}^r_{n\zeta\xi}(\omega) = \int_0^T dt\, e^{i\omega t} B^r_{n\zeta\xi}(t) \exp\left(-\gamma^2 t^2/2\right)$, with $\gamma = 0.04E_h\hbar^{-1}$ and $T \approx 100\hbar E_h^{-1}$, sufficient to converge the results (namely, the results are unchanged for smaller values of γ larger and/or larger values of T). For higher values of N_η used to test for convergence with respect to this parameter, the total propagation time was longer and the damping factor was smaller, such that $T \approx 4/\gamma$.

In the left panel of Fig. 1 we illustrate, using the Benzene molecule, the convergence of the QP energy as a function of the number N_ζ of stochastic orbitals $\zeta(\boldsymbol{r})$ (used for representing the Green's function) for different values of N_η, the number of stochastic orbitals $\eta(\boldsymbol{r})$ (used for the RPA screening calculation). For this molecule, $N_\zeta = 6000$ and $N_\eta = 8$ are sufficient to converge the QP energy to within ± 0.01 eV. Note that as N_η increases the convergence towards the final QP value is reached after a smaller number of N_ζ stochastic orbitals. The right panel of Fig. 1 provides a graphic representation of the self-consistent solution of Eq. (7) as the intersect between ε^{QP} and $\varepsilon^{KS} + \Sigma\left(\varepsilon^{QP}\right) - V_{XC}$. Note that the energy dependence of $\Sigma\left(\varepsilon^{QP}\right)$ is smooth, however, small changes in its functional form affect the value self consistent solution forε^{QP}.

The sGW QP hole energies for a subset of the GW 100 benchmark are summarized and compared to experiment and to values of the QuantumEspresso/WEST GW code in Table I and in Fig. 2. The calculations with the WEST code were based on an LDA starting point obtained from the QuantumEspresso program[40] using Troullier-Martins pseudopotentials.[39] The KS-DFT eigenvalues were converged to $\approx 10^{-3}$ E$_\mathrm{h}$. The QP energies calculated in the WEST code were subsequently converged to $\approx 5 \cdot 10^{-4}$ E$_\mathrm{h}$. Experimental geometries were taken from the NIST database[41]

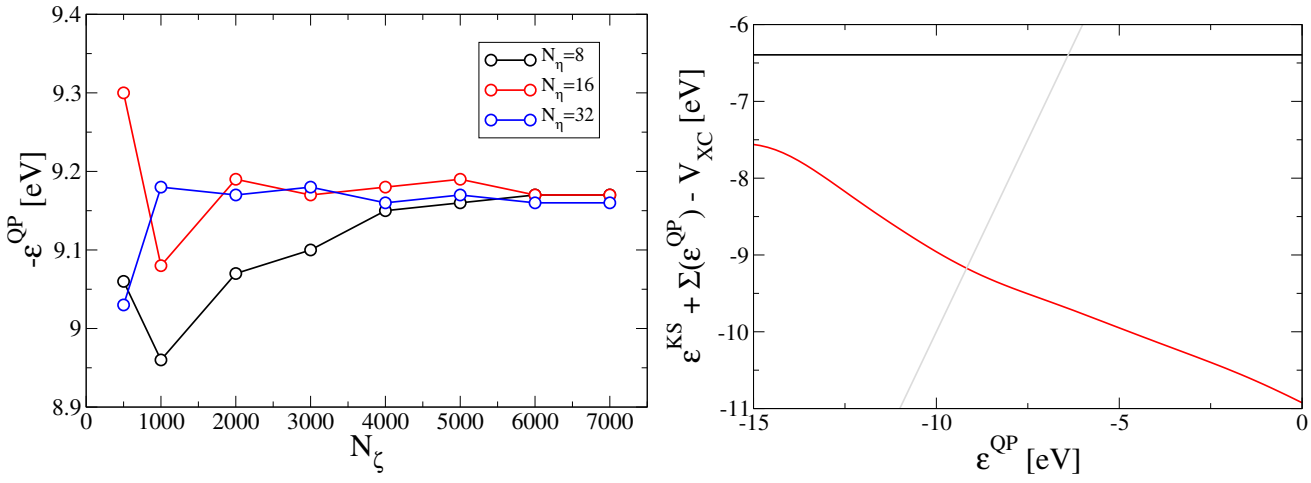

FIG. 1. Left panel: Convergence of the sGW estimate of the QP hole energy for a benzene molecule as a function of N_ζ for different values of N_η. Right: A graphic representation of the self-consistent solution of Eq. (7) for $-IP = \varepsilon^{QP}$ of benzene. The solid red line represent the right hand side of Eq. (7). The intersect with the solid grey line represents the self-consistent solution. For reference, we also depict ε^{KS} (solid black line).

System	Exp	WEST	sGW	LDA	h [a_0]	N_ζ
benzene	9.2	9.2	9.2	6.5	0.30	6000
cyclooctatetraene	8.4	8.3	8.3	5.5	0.35	6000
acetaldehyde	10.2	10.0	9.9	6.1	0.30	8000
water	12.6	12.4	12.1	7.4	0.25	6000
phenol	8.8	8.5	8.5	5.8	0.35	9000
urea	10.2	9.8	9.7	6.1	0.30	11000
methane	14.4	14.3	14.1	9.5	0.40	10000
nitrogen	15.6	15.4	15.1	10.5	0.35	7000
ethylene	10.7	10.6	10.4	6.9	0.35	12000
pyridine	9.5	9.5	9.4	6.1	0.35	7000

TABLE I. Experimental vertical ionization energies (eV) and the corresponding G_0W_0@LDA estimates for a subset of the GW 100 set.[30] The sGW QPs are compared to those of the WEST code[13] for the same pseudopotentials and grid parameters. The grid spacing h and number of $\zeta(\boldsymbol{r})$ stochastic orbitals are indicated.

and were used for all the systems investigated. To compare the numerical values across different approaches to the G_0W_0 approximation, we performed additional calculations with the QuantumEspresso/WEST code.[13,40]

Overall, the agreement between the sGW and WEST results is excellent with a mean absolute deviation of 0.13 eV. The sGW results are consistently slightly below those of WEST. However, for this set of molecules, the mean deviation is smaller than the value typically found when comparing different GW codes.[13] The largest deviation observed is 0.3 eV, for water and nitrogen. As we do not make any essential approximations beyond the numerical convergence parameters (N_ζ, N_ξ and N_η as well as T, γ and Δt) and we have carefully tested convergence with respect to these, we have no clear understanding of the reasons for the observed deviation.

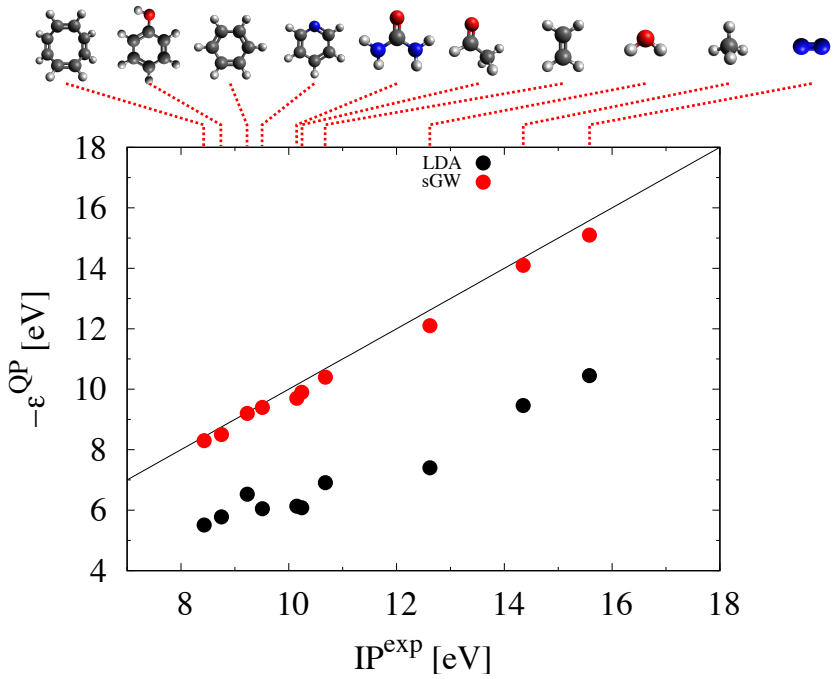

FIG. 2. Ionization potentials as predicted by various calculations (see legend) for the set of molecules listed in Tab.I are plotted against experimental values. Each molecule is depicted above the graph and dotted red line points to its experimental ionization potential on the horizontal axis. The sketches of the individual molecules use black, white, blue and red spheres to indicate positions of C, H, N and O atoms respectively. LDA results that served as a starting point for the calculations are shown by black circles. G_0W_0 results are given by filled red circles. The black line represents the one-to-one correspondence to experimental values.

IV. SUMMARY

We have reviewed in detail the sGW method presented in Ref. 28 and the numerical implementation of the approach. A comparison of the sGW approach for the hole QP energies of a subset of molecules taken from the GW 100 database[30] to results based on the GW WEST code,[13] shows close agreement of the two. The mean absolute deviation between sGW and WEST is $\approx 0.13\,\mathrm{eV}$, smaller than the typical deviation obtained for different GW codes.[30] Both sGW and WEST agree well with experimental ionization potentials. While sGW systematically slightly underestimates the IPs, the overall agreement with WEST and experiments reconfirms the validity of the stochastic algorithm, even for small molecules. Since the sGW scales nearly linearly with the system size,[28] it is the method of choice for QP excitations in extended systems with thousands of electrons.

ACKNOWLEDGMENTS

This work was supported by the Center for Computational Study of Excited-State Phenomena in Energy Materials at the Lawrence Berkeley National Laboratory, which is funded by the U.S. Department of Energy, Office of Science, Basic Energy Sciences, Materials Sciences and Engineering Division under Contract No. DE-AC02-05CH11231, as part of the Computational Materials Sciences Program. We also acknowledge support from the Israel Science Foundation – FIRST Program (Grant No. 1700/14). Part of the calculations were performed as part XSEDE computational project TG-CHE160092.[42]

---

* eran.rabani@berkeley.edu
† dxn@chem.ucla.edu
‡ roi.baer@huji.ac.il
§ Most of this work was done while at Fritz Haber Center for Molecular Dynamics, Institute of Chemistry, The Hebrew University of Jerusalem, Jerusalem 91904, Israel

[1] Hohenberg, P.; Kohn, W. Inhomogeneous Electron Gas. *Phys. Rev.* **1964**, *136*, B864.
[2] Kohn, W.; Sham, L. J. Self-Consistent Equations Including Exchange and Correlation Effects. *Phys. Rev.* **1965**, *140*, A1133.
[3] VandeVondele, J.; Borstnik, U.; Hutter, J. r. Linear scaling self-consistent field calculations with millions of atoms in the condensed phase. *J. Chem. Theory Comput.* **2012**, *8*, 3565–3573.
[4] Steinbeck, L.; Rubio, A.; Reining, L.; Torrent, M.; White, I.; Godby, R. Enhancements to the GW space-time method. *Comput. Phys. Commun.* **1999**, *125*, 05–118.
[5] Shishkin, M.; Kresse, G. Self-consistent GW calculations for semiconductors and insulators. *Phys. Rev. B* **2007**, *75*, 235102.
[6] Rostgaard, C.; Jacobsen, K. W.; Thygesen, K. S. Fully self-consistent GW calculations for molecules. *Phys. Rev. B* **2010**, *81*, 085103.
[7] Foerster, D.; Koval, P.; Sánchez-Portal, D. An O (N3) implementation of Hedin's GW approximation for molecules. *J. Chem. Phys.* **2011**, *135*, 074105.
[8] Deslippe, J.; Samsonidze, G.; Strubbe, D. A.; Jain, M.; Cohen, M. L.; Louie, S. G. BerkeleyGW: A massively parallel computer package for the calculation of the quasiparticle and optical properties of materials and nanostructures. *Comput. Phys. Commun.* **2012**, *183*, 1269 – 1289.
[9] Marom, N.; Caruso, F.; Ren, X.; Hofmann, O. T.; Körzdörfer, T.; Chelikowsky, J. R.; Rubio, A.; Scheffler, M.; Rinke, P. Benchmark of GW methods for azabenzenes. *Phys. Rev. B* **2012**, *86*, 245127.
[10] Caruso, F.; Rinke, P.; Ren, X.; Scheffler, M.; Rubio, A. Unified description of ground and excited states of finite systems: The self-consistent GW approach. *Phys. Rev. B* **2012**, *86*, 081102.
[11] van Setten, M.; Weigend, F.; Evers, F. The GW-Method for Quantum Chemistry Applications: Theory and Implementation. *J. Chem. Theory Comput.* **2012**, *9*, 232–246.
[12] Pham, T. A.; Nguyen, H.-V.; Rocca, D.; Galli, G. GW calculations using the spectral decomposition of the dielectric matrix: Verification, validation, and comparison of methods. *Phys. Rev. B* **2013**, *87*, 155148.
[13] Govoni, M.; Galli, G. Large scale GW calculations. *Journal of chemical theory and computation* **2015**, *11*, 2680–2696.
[14] Kaplan, F.; Harding, M. E.; Seiler, C.; Weigend, F.; Evers, F.; van Setten, M. J. Quasi-Particle Self-Consistent GW for Molecules. *J. Chem. Theory Comput.* **2016**,
[15] Heyd, J.; Scuseria, G. E.; Ernzerhof, M. Hybrid functionals based on a screened Coulomb potential. *J. Chem. Phys.* **2003**, *118*, 8207–8215.
[16] Baer, R.; Livshits, E.; Salzner, U. Tuned Range-separated hybrids in density functional theory. *Annu. Rev. Phys. Chem.* **2010**, *61*, 85–109.
[17] Kronik, L.; Stein, T.; Refaely-Abramson, S.; Baer, R. Excitation Gaps of Finite-Sized Systems from Optimally Tuned Range-Separated Hybrid Functionals. *J. Chem. Theory Comput.* **2012**, *8*, 1515–1531.

[18] Neuhauser, D.; Rabani, E.; Cytter, Y.; Baer, R. Stochastic Optimally Tuned Range-Separated Hybrid Density Functional Theory. *J. Phys. Chem. A* **2015**, *120*, 3071–3078.

[19] Hedin, L. New Method for Calculating the One-Particle Green's Function with Application to the Electron-Gas Problem. *Phys. Rev.* **1965**, *139*, A796–A823.

[20] Hybertsen, M. S.; Louie, S. G. First-principles theory of quasiparticles: calculation of band gaps in semiconductors and insulators. *Phys. Rev. Lett.* **1985**, *55*, 1418.

[21] Hybertsen, M. S.; Louie, S. G. Electron correlation in semiconductors and insulators: Band gaps and quasiparticle energies. *Phys. Rev. B* **1986**, *34*, 5390–5413.

[22] Aryasetiawan, F.; Gunnarsson, O. The GW method. *Rep. Prog. Phys.* **1998**, *61*, 237–312.

[23] Onida, G.; Reining, L.; Rubio, A. Electronic excitations: density-functional versus many-body Green's-function approaches. *Rev. Mod. Phys.* **2002**, *74*, 601–659.

[24] Friedrich, C.; Schindlmayr, A. Many-body perturbation theory: the GW approximation. *NIC Series* **2006**, *31*, 335.

[25] Rohlfing, M.; Louie, S. G. Electron-hole excitations and optical spectra from first principles. *Phys. Rev. B* **2000**, *62*, 4927–4944.

[26] Benedict, L. X.; Puzder, A.; Williamson, A. J.; Grossman, J. C.; Galli, G.; Klepeis, J. E.; Raty, J.-Y.; Pankratov, O. Calculation of optical absorption spectra of hydrogenated Si clusters: Bethe-Salpeter equation versus time-dependent local-density approximation. *Phys. Rev. B* **2003**, *68*, 085310.

[27] Tiago, M. L.; Chelikowsky, J. R. Optical excitations in organic molecules, clusters, and defects studied by first-principles Green function methods. *Phys. Rev. B* **2006**, *73*, 205334.

[28] Neuhauser, D.; Gao, Y.; Arntsen, C.; Karshenas, C.; Rabani, E.; Baer, R. Breaking the Theoretical Scaling Limit for Predicting Quasiparticle Energies: The Stochastic G W Approach. *Phys. Rev. Lett.* **2014**, *113*, 076402.

[29] Rabani, E.; Baer, R.; Neuhauser, D. Time-dependent stochastic Bethe-Salpeter approach. *Phys. Rev. B* **2015**, *91*, 235302.

[30] van Setten, M. J.; Caruso, F.; Sharifzadeh, S.; Ren, X.; Scheffler, M.; Liu, F.; Lischner, J.; Lin, L.; Deslippe, J. R.; Louie, S. G.; Yang, C.; Weigend, F.; Neaton, J. B.; Evers, F.; Rinke, P. GW 100: Benchmarking G 0 W 0 for Molecular Systems. *J. Chem. Theory Comput.* **2015**, *11*, 5665–5687.

[31] Nguyen, H.-V.; Pham, T. A.; Rocca, D.; Galli, G. Improving accuracy and efficiency of calculations of photoemission spectra within the many-body perturbation theory. *Phys. Rev. B* **2012**, *85*, 081101.

[32] Baer, R.; Neuhauser, D.; Rabani, E. Self-Averaging Stochastic Kohn-Sham Density-Functional Theory. *Phys. Rev. Lett.* **2013**, *111*, 106402.

[33] Neuhauser, D.; Baer, R.; Rabani, E. Communication: Embedded fragment stochastic density functional theory. *J. Chem. Phys.* **2014**, *141*, 041102.

[34] Hutchinson, M. F. A stochastic estimator of the trace of the influence matrix for Laplacian smoothing splines. *Communications in Statistics-Simulation and Computation* **1990**, *19*, 433–450.

[35] Baer, R.; Head-Gordon, M. Chebyshev expansion methods for electronic structure calculations on large molecular systems. *J. Chem. Phys.* **1997**, *107*, 10003–10013.

[36] Baer, R.; Head-Gordon, M. Sparsity of the density matrix in Kohn-Sham density functional theory and an assessment of linear system-size scaling methods. *Phys. Rev. Lett.* **1997**, *79*, 3962–3965.

[37] Fetter, A. L.; Walecka, J. D. *Quantum Thoery of Many Particle Systems*; McGraw-Hill: New York, 1971; p 299.

[38] Gao, Y.; Neuhauser, D.; Baer, R.; Rabani, E. Sublinear scaling for time-dependent stochastic density functional theory. *J. Chem. Phys.* **2015**, *142*, 034106.

[39] Troullier, N.; Martins, J. L. Efficient Pseudopotentials for Plane-Wave Calculations. *Phys. Rev. B* **1991**, *43*, 1993–2006.

[40] Giannozzi, N.; Baroni, S.; Bonini, N.; Calandra, M.; Car, R.; Cavazzoni, C.; Ceresoli, D.; Chiarotti, G.; Cococcioni, M.; Dabo, I.; et al. QUANTUM ESPRESSO: a modular and open-source software project for quantum simulations of materials. *Journal of physics: Condensed matter* **2009**, *21*, 395502.

[41] NIST Computational Chemistry Comparison and Benchmark Database NIST Standard Reference Database Number 101 Release 18, October 2016, Editor: Russell D. Johnson III http://cccbdb.nist.gov/,.

[42] Towns, J.; Cockerill, T.; Dahan, M.; Foster, I.; Gaither, K.; Grimshaw, A.; Hazlewood, V.; Lathrop, S.; Lifka, D.; Peterson, G.;et al. XSEDE: accelerating scientific discovery. *Computing in Science & Engineering* **2014**, *16*, 62–74.